myotonic dystrophy. The pUC19-based plasmids (pRW plasmids) used were derived from pSH1 and pSH2, containing 75 and 130 repeats of CTG, respectively (*14*). The DNA was cleaved with restriction endonucleases, and one end of the DNA was labeled with streptavidin. The length of the segment occupied by the triplet repeats, measured as a percentage of the distance from the labeled end for the $(CTG)_{250}$ insert in pRW3222 was 46 to 72%, 50 to 70% for the $(CTG)_{180}$ insert in pRW3219, 53 to 68% for the $(CTG)_{130}$ insert in pRW1981, 56 to 66% for the $(CTG)_{75}$ insert in pRW1980, 58 to 64% for the $(CTG)_{50}$ insert in pRW3213, 60 to 64% for the $(CTG)_{26}$ insert in pRW3212, and 32 to 43% for the $(CTG)_{130}$ insert in pSH2. In the figures, positions along the DNA are indicated as map units with each percentage point equal to 1 map unit.

13. Y.-H. Wang and J. D. Griffith, in preparation.
14. S. Amirhaeri, Y.-H. Wang, R. D. Wells, J. D. Griffith, unpublished data.
15. DNA polymerase pausing studies and physical determinations on these plasmids reveal a base pair repeat periodicity of 12 + 9 (2 × 10.5; the helical repeat of B-form DNA is 10.5 base pairs) and longer range conformational effects that may enhance nucleosome formation (S. Kang, K. Ohshima, S. Amirhaeri, R. D. Wells, in preparation).
16. We incubated closed circular plasmids in 5 mM $MgCl_2$ at 55°C for 30 min before we mixed the DNA with purified calf thymus histone octamers (*9*) in a buffer containing 2 M NaCl. The amount of histone was experimentally determined to result in an average of one nucleosome per DNA strand. We slowly lowered the NaCl concentration by dilution to 0.6 M to form stable nucleosomes. The nucleosome-assembled DNA was fixed with 0.6% glutaraldehyde for 10 min at 21°C, chromatographed over 1 ml of Sephadex G-50 (Pharmacia), and then treated with Bsa HI and Sca I restriction enzymes (pSH2) or Bsr FI and Alw NI (pRW3222). We labeled only the Bsa HI (or Bsr FI) ends of the molecules with biotinylated deoxycytidine 5′-triphosphate using the large fragment of DNA polymerase; this end was then labeled with streptavidin.
17. DNA-histone complexes prepared as described (*16*) were mixed with a buffer containing 2 mM spermidine and applied to carbon foils treated with a high-voltage discharge in a mild vacuum to introduce charged groups on the surface to facilitate DNA binding, and complexes were processed for EM as described [J. D. Griffith and G. Christiansen, *Annu. Rev. Biophys. Bioeng.* **7**, 19 (1978)]. We analyzed only those DNAs with a single nucleosome to avoid errors resulting from the progressive compaction of DNAs with multiple nucleosomes.
18. N. C. Stellwagen, *Biochemistry* **22**, 6186 (1983); G. Muzard, B. Theveny, B. Revet, *EMBO J.* **9**, 1289 (1990).
19. The percent values above the black bars represent the fraction of nucleosomes present in the repeat blocks. Dividing this number by the average fraction of nucleosomes occupying a segment equal in size to the repeat block (from the flanking regions) gave a value (in parentheses) representing the efficiency of nucleosome assembly for the CTG repeat block, as compared with the flanking regions.
20. To compare the efficiency of nucleosome assembly for the plasmids in Fig. 3, we normalized the values from the black bars by subtracting the percentage background assembly. For example, 55% (0.55) of all the nucleosomes assembled on the plasmid containing a $(CTG)_{180}$ block (Fig. 3B) localized to the block $(CTG)_{180}$, which encompasses 20% (0.20) of the total plasmid length. Thus, the length-normalized assembly for the plasmid containing a $(CTG)_{180}$ block is 0.35 (0.55 to 0.20). These length-normalized assembly values were plotted against the CTG copy number. Bars represent the range of the values derived from dividing the DNA segment into 10, 20, 50, or 100 divisions. Curve was fit with a French curve. A DNA sequence containing no CTG repeats or other nucleosome positioning sequences has a length-normalized assembly value equal to zero.
21. We thank C. T. Caskey (Baylor College of Medicine) for the human myotonic dystrophy cDNA.

Supported by grants from NIH (GM31819 and GM42342) and the ACS (NP583) (J.D.G.) and by grants from NIH (GM 30822), NSF (86-07785), and the Robert A. Welch Foundation (R.D.W.).

29 March 1994; accepted 8 June 1994

# Pf1 Virus Structure: Helical Coat Protein and DNA with Paraxial Phosphates

David J. Liu and Loren A. Day

**The helical path of the DNA in filamentous bacteriophage Pf1 was deduced from different kinds of existing structural information, including results from x-ray fiber diffraction. The DNA has the same pitch, 16 angstroms, as the surrounding helix of protein subunits; the rise and rotation per nucleotide are 6.1 angstroms and 132 degrees, respectively; and the phosphates are 2.5 angstroms from the axis. The DNA in Pf1 is, therefore, the most extended and twisted DNA structure known. On the basis of the DNA structure and extensive additional information about the protein, a model of the virion is proposed. In the model, the DNA bases reach out, into the protein, and the lysine and arginine side chains reach in, between the DNA bases, to stabilize the paraxial phosphate charges; the conformation of the protein subunit is a combination of α and $3_{10}$ helices.**

The Pf1 virus is 2 μm long and contains a circular single-stranded DNA of 7349 nucleotides wrapped in a coat of protein subunits (*1–3*). This virus stands out among all filamentous bacteriophage (all species of the genus *Inovirus*) in having the highest axial distance, about 6 Å, between two nucleotides (*3, 4*) and an integer nucleotide/subunit ratio (n/s) of 1 (*5, 6*). This is the lowest n/s value of all known DNA-protein complexes. Structural data for Pf1 are available from spectroscopic methods (*5–15*), ion probes of its DNA (*16*), chemical modification of its protein (*17, 18*), x-ray fiber diffraction (*18, 19*), and neutron diffraction (*20*). Structural models for the major coat protein of Pf1 virus have been proposed (*20–22*), but heretofore, no model of the entire virion has been presented that contains DNA and systematically accounts for all relevant data, including the x-ray diffraction results for the DNA. The problem has been that the apparent structural repeat in x-ray fiber diffraction patterns for Pf1 calls for odd numbers of subunits (*5, 18, 23*), yet the unit stoichiometry (n/s = 1) calls for an even number. Specifically, the stoichiometry implies that each protein subunit directly contacts one nucleotide, either up-strand or down-strand; hence, there are two types of protein subunit and an even total number of protein subunits in a true repeat. In this paper, we provide a solution that establishes the symmetry of the DNA helix and places the phosphates close to the axis (paraxial). Working outward from the phosphates and making use of experimental (*4–19, 24*) and theoretical (*25–27*) results, we have developed models for the DNA and for the protein of Pf1 virus.

The establishment of the symmetry of any macromolecular assembly, such as a virus, is the critical step in solving its structure. In the case of a filamentous virus, it is the establishment of the helical symmetries of both its DNA and its protein coat. The x-ray fiber diffraction data for Pf1 have established the approximate helical symmetry of the coat, showing that the protein subunits are uniformly oriented with respect to the structural axis (*18, 19*). Information relating to DNA symmetry has been from the $^{31}P$ solid-state nuclear magnetic resonance (NMR) spectrum of oriented Pf1, from which it was concluded that the phosphates of both strands are "uniformly oriented" with respect to the structural axis (*10*). We have found that information on DNA symmetry is also in the x-ray diffraction data. On the basis of the protein coat symmetry, an electron density map for the entire structure was calculated (*19*). In the map, there are three spots of high density at radial positions below 10 Å. Our integration of the electron density above 0.6 $e/Å^3$ in these spots yielded 25 electrons, and the number of electrons in the largest spot approximates the sum for the two smaller spots. The maximum electron density in the spots exceeds 1.4 $e/Å^3$, which is too high for water but is appropriate for phosphate. There are 31 electrons in one O–P–O group (phosphorus and the two nonesterified oxygen atoms). The largest spot has the shape of a tilted O–P–O group. These spots are not from protein or solvent, so they must be from DNA.

Diffraction patterns contain information

Public Health Research Institute, 455 First Avenue, New York, NY 10016, USA.

on the ordered components. A reverse transform of a diffraction pattern retains all, and only, the information from the components that follow the symmetry assumed. The reverse transform based on an asymmetric unit containing one protein subunit generates, apparently, two O–P–O groups, each having half the electrons of one O–P–O group. Because of this, the apparent electron density for two O–P–O groups must follow the protein coat symmetry, and because the number of nucleotides in each strand is half the total number of protein subunits (n/s = 1), the nucleotides in a given strand must occupy every other position in the Pf1 helix. The x-ray fiber diffraction pattern of Pf1 virus shows an apparent repeat of 71 protein subunits in 13 turns axially spanning 216.5 Å, so a cross-sectional slice 3.05 Å thick represents the asymmetric unit (*18, 19*). For the protein coat helix, the rise per subunit ($z_{SU}$) is 3.05 Å, and the rotation ($\phi_{SU}$) is 65.92°. Thus, the rise per nucleotide in each DNA strand ($z_{DNA}$) is 6.1 Å, and the rotation ($\phi_{DNA}$) is 131.84°. The axial and azimuthal displacements relating the two strands can be deduced. The azimuthal displacements between the larger spot and the two smaller spots are the same, just under 120° [figure 1 of (*19*)].

Averaged over a 0.76 Å slice [figure 1 of (*28*)], the density in the upper left spot is higher than the density averaged over the 3.05 Å slice, so it represents density of positive axial displacement relative to that of the larger spot in the 3.05 Å slice. Further comparison of these two maps at different resolution also suggests the axial positions of the two oxygen atoms and an O–P–O plane tilt of about 25° ± 10°. Electrostatic free energy calculations (*27*) dictate an evenly spaced arrangement for the charges that relates the two antiparallel strands by an axial translation, $z_{inter}$, of 3.05 Å, and an azimuthal rotation, $\phi_{inter}$, of −114.08° (= 65.92° − 180°) (Fig. 1A).

On the basis of this lattice, the upper left spot was translated +3.05 Å, and the upper right spot, −3.05 Å, relative to the largest spot, and then, a three-dimensional map (Fig. 1B) was generated according to the procedure given in (*19*). In the z direction, there is one nucleotide every 3.05 Å, one from one strand, the next from the other strand. Conceptually, if one strand were rotated about the structural axis by π (180°), all of the O–P–O groups in the two strands would form a single helix, following the protein coat helix exactly (*29*). The radial positions of the phosphorus atoms are about 2.5 Å. Thus, the fundamental symmetry of the Pf1 DNA helix is established.

Having the O–P–O groups and hence the backbone set, we move out to sugar rings and bases. In this region, the electron density is relatively low and smooth because all of the sugars and the bases are

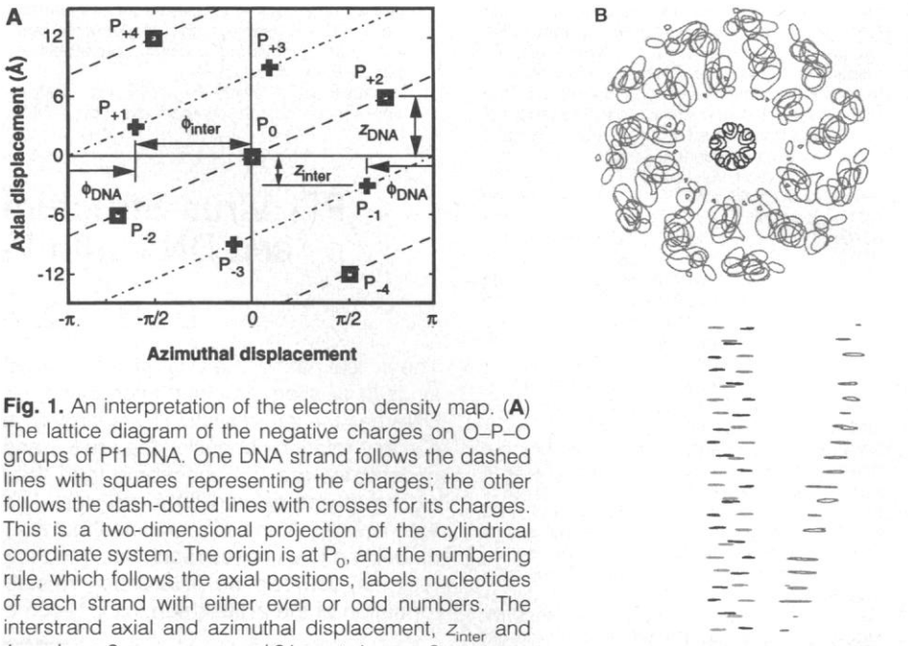


**Fig. 1.** An interpretation of the electron density map. (**A**) The lattice diagram of the negative charges on O–P–O groups of Pf1 DNA. One DNA strand follows the dashed lines with squares representing the charges; the other follows the dash-dotted lines with crosses for its charges. This is a two-dimensional projection of the cylindrical coordinate system. The origin is at $P_0$, and the numbering rule, which follows the axial positions, labels nucleotides of each strand with either even or odd numbers. The interstrand axial and azimuthal displacement, $z_{inter}$ and $\phi_{inter}$, have $2z_{inter} = z_{DNA}$ and $2\phi_{inter} + \phi_{DNA} = 2\pi$, so $z_{inter} = z_{DNA}/2$ and $\phi_{inter} = \pi - \phi_{DNA}/2$. The plot of $\phi_{DNA}$, measured between $P_{-1}$ and $P_1$, is shown in two parts. For the protein coat helix, $z_{SU} = z_{DNA}/2$ and $\phi_{SU} = \phi_{DNA}/2$. Assigning $P_0(r,0,0)$, we have $P_1(r,\phi_{SU}-\pi,z_{SU})$, so the DNA symmetry is expressed in the parameters of the protein helix [see also (*27*)]. (**B**) A top view of a 21.35 Å section of the map (top), and a side view of a 67.1 Å section (bottom). In the side view, two strands of DNA and only one protein subunit are shown. The density at the center is from the O–P–O groups. These images were constructed by translating and rotating the 3.05 Å slice (*19*) after the axial positions of the two smaller spots for DNA had been restored (see text). The side views were tilted by 5°.

not the same. A reverse transform process based on $l = 13n + 71m$ discards diffraction from these parts as noise (*30*), so this region has electron density between 0.4 and 0.6 $e/Å^3$, which is near the average (*31*). The DNA backbone constrains the location of sugar rings, but their configurations may vary depending on the orientation of the strand and the particular base. On the basis of Raman spectra (*13*), a C2′ endo/anti sugar configuration is assigned. Spectroscopic studies indicate that the bases are not stacked (*6, 7*). They tilt away significantly (at least 60°) from being perpendicular to the structural axis (*8, 12*). In an aqueous environment, they are accessible to $Ag^+$ and $Hg^{2+}$ (*16*) and are in a position to interact with $Tyr^{40}$ of the coat protein (*6, 7, 11*). The bases point away from the structural axis. The DNA model is shown in Fig. 2A.

We now move out to the protein subunit (Fig. 2B). Spectroscopic data show exclusively helical coat protein, probably a combination of α helix (*6, 9, 12*) and some $3_{10}$ helix (*6*). We modeled the structure as a continuously helical protein of α- and $3_{10}$-helical segments, following the shape given by the electron density data (Fig. 1B). The {ϕ,Ψ} angles of the helices vary within a range of ±5° (*32*). We began with the COOH-terminal α-helical segment and set its orientation by putting $Arg^{44}$ and $Lys^{45}$ on the inner side, facing the DNA. The quenched fluorescence of $Tyr^{40}$ suggests that it interacts with the DNA bases (*7, 11*), so the phenol group was made accessible to the bases through edge-on hydrogen bonding, rather than through base-tyrosine stacking (*14*). The radial positions of deuterium labels of $Tyr^{40}$ and $Met^{42}$ (*20*) further constrain the orientation of the COOH terminus. A theoretical study of *Inovirus* subunit packing predicted a junction between the inner and outer layer segments near residue 26 (*26*). The electron density map shows a smooth turn in this region. Variations in the {ϕ,Ψ} angles allow the backbone to shift smoothly from inner layer to outer layer. Glycines, which terminate α helices at a high frequency and favor $3_{10}$-helix formation (*32*), occur at residues 23, 24, and 28. Therefore, we connected the inner segment of α helix from $Ala^{29}$ through $Ala^{46}$ to the outer segment from $Gly^1$ through $Ile^{22}$ with two turns of $3_{10}$ helix from $Gly^{23}$ through $Gly^{28}$. The electron density map also shows another bend near $Gly^{15}$, so one turn of $3_{10}$ helix from $Gly^{15}$ through $Gly^{17}$ was used to control the orientation of the $NH_2$ terminus in the otherwise α-helical outer segment. Solid-state NMR results indicate that the nitrogen atoms of $Gly^1$ and at least one of $Gly^{15}$ and $Gly^{17}$ are mobile (*15*). In our

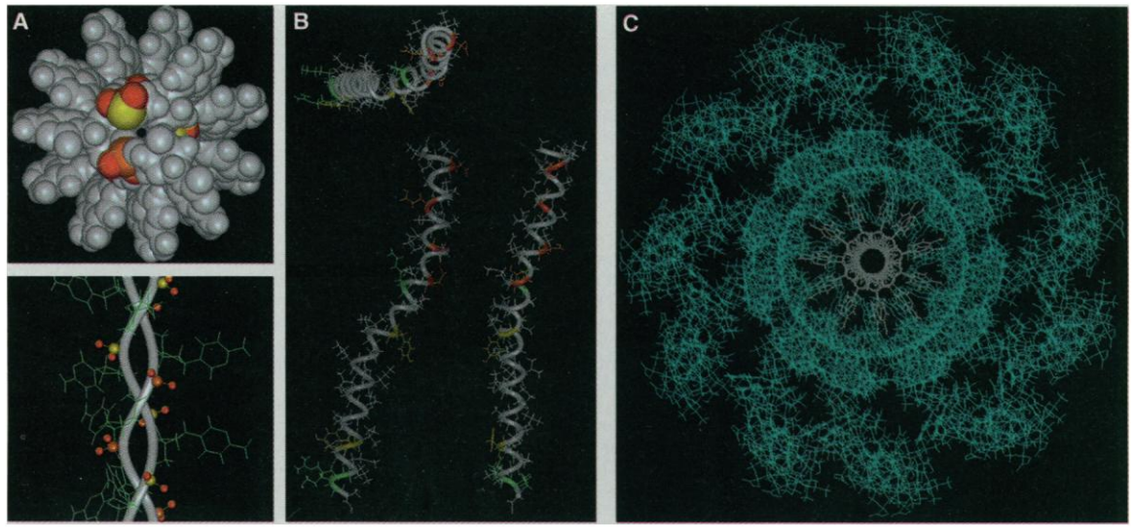


**Fig. 2.** Structure models for Pf1 virus (PDB accession number of coordinates: 1PFI). (**A**) The model of Pf1 DNA. The base used for this model is cytosine. The second strand is generated from the first by means of a twofold rotation around the *x* axis, assigned as a radius through a P atom, followed by a translation in the *z* direction of 3.05 Å and a rotation of −114.08° around the *z* axis. In the side view (bottom), the O–P–O groups from both strands are shown at 30% of their van der Waals radii. Despite their up- and down-strand difference, the O–P–O groups from the two strands have the same orientation relative to the structural axis. (**B**) Protein model in three views: top (upper), side (lower left), and back (lower right). The protein faces DNA to the left in the side view. The backbone is traced with ribbons, and charged residues and tyrosines are colored. The sequence is GVIDTSAVESAITDGQGDMKAIGGYIVGALVILAVAGLIYSMLRKA (*2, 34*). (**C**) A top view of the Pf1 virus model showing a 67 Å section of 11 structural units, each consisting of two nucleotides and their associated protein subunits. About 50% of the total volume is occupied by solvent molecules. Side chains of $Lys^{44}$ and $Arg^{45}$ reach into the region of DNA to neutralize the charges on the DNA backbone; the phenolic ring of $Tyr^{40}$ is in a position to interact with the bases.

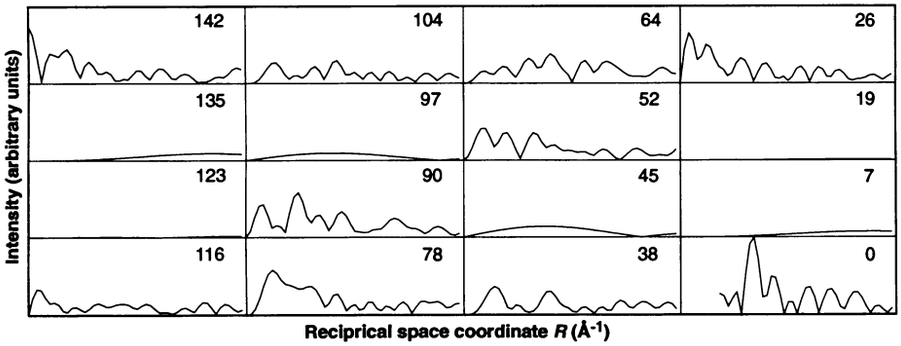


**Fig. 3.** Layer lines of the diffraction pattern that provide information on DNA calculated from the model of Pf1 virus. Bessel functions were calculated up to 50th order, and only layer lines with contributions from Bessels $J_0$ through $J_4$ are shown. The reciprocal space coordinate *R* is at a scale of 0 to 0.25 $Å^{-1}$. Layer lines are numbered according to the selection rule $l = 26n + 71m$, where there are 71 asymmetric units, each containing two nucleotides and two protein subunits. The fit to observed diffraction on even-number layer lines is comparable to the fit obtained by others for another model (*22*). The diffraction on odd-number layer lines is from the O–P–O groups only. No intensity has been predicted on layer lines with Bessel functions of even order, for example, layer lines 19 and 123 (*29*).

model, $Gly^1$ and $Gly^{15}$ are on the surface of the virion, with little restriction to their motion. The axial length of this protein model is 65 Å, in accord with the length of 63 to 66 Å from the electron density map.

The radial positions of valine, isoleucine, methionine, and tyrosine residues in the model have been optimized to fit the radial positions of difference peaks from neutron diffraction (*20*). The average radial discrepancy between our model and the data is 1.2 Å, whereas another model having a nonhelical "loop" of seven residues (*20*) has a corresponding discrepancy of 2.7 Å (*33*). The "loop" model (*20, 21*) contradicts the electron density map because its contour length is too short; it also contradicts various spectroscopic data, which call for exclusively helical protein. Thus, we consider the "loop" model to be incorrect. Our introduction of $3_{10}$ helices has produced a model that fits the length, all of the spectroscopic data, and the neutron diffraction data. So that our model would fit chemical modification results (*17*), the configurations of the side chains were adjusted; for example, the side chains of $Asp^{14}$ and $Asp^{18}$ are not on the surface of the virion and may be hydrogen bonded to neighboring groups. Both $Tyr^{25}$ and $Tyr^{40}$ are in hydrophobic environments, as suggested by analysis of their absorbance in the ultraviolet (6), and $Tyr^{25}$ is near the surface of the virion (*17, 18*). The model was constructed to follow the electron density map based on x-ray fiber diffraction data at 4 Å resolution (*19*), so the protein part fits these diffraction data. The predicted contributions from DNA to the diffraction also fit the data, without problems on any prohibited layer lines (Fig. 3).

Upon dissociation of the virion, the conformations of the DNA and the coat protein in intact Pf1 virus become lost (6). There exists no such everted DNA conformation without its protein shell, and there exists no such highly helical protein conformation without the DNA backbone. The components in the virion are held together tightly—as a result of the covalently continuous DNA backbone, its electrostatic interactions with the protein shell (*27*), and the hydrophobic interactions between protein subunits—but the structure remains flexible (*4*). Local adjustments that would optimize the electrostatics and the hydrogen bonding between protein and individual bases would not require substantial modifications in other parts of the protein structure. Although the structure is simple, its assembly requires a complex set of reactions at the cell membrane, as is true of all members of the genus *Inovirus*. Substantial changes in secondary structure occur during the assembly; the flexibility that glycine brings to the coat protein may play an important role in these changes.

## REFERENCES AND NOTES

1. K. Takeya and K. Amako, *Virology* **28**, 163 (1966).
2. D. F. Hill *et al.*, *J. Mol. Biol.* **218**, 349 (1991).
3. L. A. Day *et al.*, *Annu. Rev. Biophys. Biophys. Chem.* **17**, 509 (1988).
4. S. A. Reisberg, thesis, New York University (1989).

5. R. L. Wiseman and L. A. Day, *J. Mol. Biol.* **116**, 607 (1977).
6. L. G. Kostrikis, D. J. Liu, L. A. Day, *Biochemistry* **33**, 1694 (1994).
7. L. A. Day, R. Wiseman, C. J. Marzec, *Nucleic Acids Res.* **7**, 1393 (1979).
8. J. Torbet and G. Maret, *Biopolymer* **20**, 2657 (1981); B. A. Clack and D. M. Gray, *ibid.* **32**, 795 (1992).
9. G. J. Thomas, B. Prescott, L. A. Day, *J. Mol. Biol.* **165**, 321 (1983); G. J. Thomas, *Spectrochim. Acta A* **41**, 217 (1985).
10. T. A. Cross, P. Tsang, S. J. Opella, *Biochemistry* **22**, 721 (1983).
11. K. O. Greulich and R. Wijnaendts van Resandt, *Biochim. Biophys. Acta* **782**, 446 (1984).
12. H. Fritzsche, P. Tsang, S. J. Opella, N. R. Kallenbach, *Stud. Biophys.* **116**, 175 (1986).
13. G. J. Thomas Jr., B. Prescott, S. J. Opella, L. A. Day, *Biochemistry* **27**, 4350 (1988).
14. A. Casadevall and L. A. Day, *ibid.*, p. 3599.
15. K.-J. Shon *et al.*, *Science* **252**, 1303 (1991).
16. A. Casadevall and L. A. Day, *Biochemistry* **22**, 4831 (1983).
17. Y. Nakashima and W. H. Konigsberg, *J. Mol. Biol.* **138**, 493 (1980).
18. C. Nave *et al.*, *ibid.* **149**, 675 (1981).
19. R. K. Bryan *et al.*, *Proc. Natl. Acad. Sci. U.S.A.* **80**, 4728 (1983).
20. W. Stark *et al.*, *J. Mol. Biol.* **199**, 171 (1988); R. Nambudripad *et al.*, *ibid.* **220**, 359 (1991).
21. R. Nambudripad, W. Stark, S. J. Opella, L. Makowski, *Science* **252**, 1305 (1991).
22. D. A. Marvin, C. Nave, M. Bansal, R. D. Hale, E. K. H. Salje, *Phase Transitions* **39**, 45 (1992).
23. L. Makowski and D. L. D. Caspar, *J. Mol. Biol.* **145**, 611 (1981).
24. The conformations of Pf1 DNA and protein differ only slightly at different temperatures according to circular dichroism (*14*). This allows us to use certain data collected at high temperature in developing a model for the low-temperature form.
25. BREAKRING and MAKERING, programs for analysis and construction of furanose rings [C. J. Marzec and L. A. Day, *J. Biomol. Struct. Dynam.* **10**, 1091 (1993)].
26. C. J. Marzec and L. A. Day, *Biophys. J.* **53**, 425 (1988).
27. ———, in preparation.
28. D. A. Marvin, R. K. Bryan, C. Nave, *J. Mol. Biol.* **193**, 315 (1987).
29. The structure factor of a helix with a repeat of $u$ units in $t$ turns, axially spanning distance $c$, is

$$F\left(R,\Psi,\frac{l}{c}\right) = \sum_{n=-\infty}^{\infty} G_{n,l}(R)e^{in(\Psi+\pi/2)} \quad (1)$$

$$G_{n,l}(R) = \sum_{j=1}^{N} f_j J_n(2\pi R r_j) e^{i}\left(\frac{2\pi l z_j}{c} - n\phi_j\right) \quad (2)$$

where $R$, $\Psi$, and $l/c$ are the reciprocal space cylindrical coordinates and $r_j$, $\phi_j$, and $z_j$ are the real space cylindrical coordinates of the $j$th of $N$ atoms, and $G$ is the part independent of $\Psi$. The permitted Bessel function of order $n$ on layer line $l$ is from the helix selection rule $l = tn + um$, where $m$ is an integer [A. Klug, F. H. C. Crick, H. W. Wyckoff, *Acta Crystallogr.* 11, 199 (1958)]. For each pair of atoms from two protein subunits $SU_0$ and $SU_1$ and two O–P–O groups $P_0$ and $P_1$, radius $r$ and diffraction factors $f$ are constant, so we define $G_0 = fJ_n(2\pi Rr)$. For the structural unit containing two protein subunits $SU_0$ $(r,0,0)$ and $SU_1$ $(r,\phi_{SU},z_{SU})$ and two nucleotides $P_0$ $(r,0,0)$ and $P_1$ $(r,\phi_{SU}-\pi,z_{SU})$

$$G = G_{DNA} + G_{SU} \quad (3)$$

$$G_{DNA} = G_{0,DNA} + G_{0,DNA}e^{i}\left[\frac{2\pi l z_{SU}}{c} - n(\phi_{SU} - \pi)\right]$$

$$= G_{0,DNA}\left[1 + (-1)^n e^{i}\left(\frac{2\pi l z_{SU}}{c} - n\phi_{SU}\right)\right] \quad (4)$$

$$G_{SU} = G_{0,SU} + G_{0,SU}e^{i}\left(\frac{2\pi l z_{SU}}{c} - n\phi_{SU}\right)$$

$$= G_{0,SU}\left[1 + e^{i}\left(\frac{2\pi l z_{SU}}{c} - n\phi_{SU}\right)\right] \quad (5)$$

The correct selection rule for Pf1 virus at low temperature is $l = 26n + 71m$, where there are 71 asymmetric subunits containing two protein subunits each, yet there are still 71 individual subunits in 13 turns. For DNA, when $n$ is an even number, the diffraction of the O–P–O groups appears as if from a helix of O–P–O groups following the protein symmetry exactly; when $n$ is an odd number, the diffraction appears to be from two such helices, thus revealing the existence of two strands.
30. It seems that even if the selection rule $l = 26n + 71m$ had been applied in the transform for an asymmetric unit containing two nucleotides and two protein subunits, not much more information would have been extracted from the diffraction patterns. Therefore, $l = 13n + 71m$ appears to be a good approximation applied to solve the structure that significantly simplified data processing while maintaining acceptable accuracy.
31. The maximum entropy calculation in the transform starts with a "flat" distribution of density (maximal entropy). It then rearranges the density according to the information from the diffraction patterns filtered through the selection rule. If the constraints obtained are not sufficient, it simply preserves much of the starting "flat" distribution.
32. L. Pauling, R. B. Corey, and H. R. Branson [*Proc. Natl. Acad. Sci. U.S.A.* **37**, 205 (1951)] predicted such secondary structure with $\{\phi,\Psi\} = \{-74°,-4°\}$; in a survey, D. J. Barlow and J. M. Thornton [*J. Mol. Biol.* **201**, 601 (1988)] found the average $\{\phi,\Psi\}$ to be $\{-71°,-18°\}$; on the basis of then available structural data, J. S. Richardson and D. C. Richardson [in *Prediction of Protein Structure and the Principles of Protein Conformation*, G. D. Fasman, Ed. (Plenum, New York, 1989), pp. 1–98] defined a $3_{10}$ helix as having $\{\phi,\Psi\}$ about $\{-70°,-5°\}$ and concluded that glycines terminate an $\alpha$ helix at a high frequency and favor a $3_{10}$ helix. We assigned $\{\phi,\Psi\}$ values on the basis of these values for a $3_{10}$ helix. For an $\alpha$ helix, the set of $\{\phi,\Psi\}$ angles is assigned as $\{-65°,-40°\}$.
33. We only used the radial positions of the labels because the axial and azimuthal positions currently available are uncertain, as a consequence of difficulties in backbone tracing (*20*).
34. Abbreviations for the amino acid residues are A, Ala; D, Asp; E, Glu; G, Gly; I, Ile; K, Lys; L, Leu; M, Met; Q, Gln; R, Arg; S, Ser; T, Thr; V, Val; and Y, Tyr.
35. We thank S. L. Chen and C. J. Marzec for discussions and R. W. Hendrix for comments on the manuscript. We have used Linux, GNU C, gnuplot, and other freely available software and are grateful to their authors, among them L. Torvalds, R. Stallman, H. J. Lu, T. Williams, and C. Kelley. This work is part of the dissertation research of D.J.L. [New York University (NYU) School of Medicine]. Financial support has been through NIH (GM42286 to L.A.D.), with partial support from the Sackler Institute, NYU.

9 February 1994; accepted 6 June 1994

# Specific Interaction of Type I Receptors of the TGF-β Family with the Immunophilin FKBP-12

Tongwen Wang, Patricia K. Donahoe, Antonis S. Zervos*

**Transforming growth factor–β (TGF-β) family members bind to receptors that consist of heteromeric serine-threonine kinase subunits (type I and type II). In a yeast genetic screen, the immunophilin FKBP-12, a target of the macrolides FK506 and rapamycin, interacted with the type I receptor for TGF-β and with other type I receptors. Deletion, point mutation, and co-immunoprecipitation studies further demonstrated the specificity of the interaction. Excess FK506 competed with type I receptors for binding to FKBP-12, which suggests that these receptors share or overlap the macrolide binding site on FKBP-12, and therefore they may represent its natural ligand. The specific interaction between the type I receptors and FKBP-12 suggests that FKBP-12 may play a role in type I receptor–mediated signaling.**

Transforming growth factor–β elicits its effects by binding to a heteromeric complex of type I and type II receptors (*1–3*). Four transmembrane serine-threonine kinases—R1, R2, R3, and R4—have been cloned (*4–11*). These are the type I receptors for members of the TGF-β family. R4 is the functional type I receptor for TGF-β (*7, 12*), and R1 and R3 both can bind activin and TGF-β when expressed with the appropriate type II receptors (*5, 6, 10, 13*). R1 mRNA is specifically localized in the mesenchyme surrounding the Müllerian duct during embryonic Müllerian duct regression, which suggests that it is a candidate type I receptor for Müllerian inhibiting substance (*4*).

To study type I receptor–mediated signaling, we used a variant of the yeast two-hybrid system (*14–16*) to identify proteins that interact with the cytoplasmic domain of R1 (R1C). The entire cytoplasmic domain of R1 was fused with the DNA binding domain of LexA to serve as the "bait" (*17*). Because R1 is expressed in heart tissue (*4*), a yeast expression complementary DNA (cDNA) library from neonatal rat heart was used for screening. Seventy-six cDNAs were isolated (*14*), partially sequenced, and grouped. The largest family, consisting of 47 cDNAs of about 1.5 kb,

T. Wang, Cutaneous Biology Research Center and Pediatric Surgical Research Laboratory, Massachusetts General Hospital, Boston, MA 02114, USA.
P. K. Donahoe, Pediatric Surgical Research Laboratory, Massachusetts General Hospital, Boston, MA 02114, USA.
A. S. Zervos, Cutaneous Biology Research Center, Massachusetts General Hospital, Charlestown, MA 02129, USA.
*To whom correspondence should be addressed.